Control Design for Optimizing Efficiency in Inductive Power Transfer Systems

Zhicong Huang, *Student Member, IEEE*, Siu-Chung Wong, *Senior Member, IEEE*, and Chi K. Tse, *Fellow, IEEE*

***Abstract*—Inductive power transfer (IPT) converters are resonant converters that attain optimal energy efficiencies for a certain load range. To achieve maximum efficiency, it is common to cascade the IPT converter with front-side and load-side dc/dc converters. The two dc/dc converters are normally controlled cooperatively for the requirements of output regulation and maximum efficiency tracking using a control technique based on perturbation and observation, which is inevitably slow in response. In this paper, a decoupled control technique is developed. The load-side dc/dc converter is solely responsible for output regulation, while the front-side converter is responsible for impedance-matching of the IPT converter by controlling its input-to-output voltage ratio. The controls are linear and therefore fast. DC and small-signal transfer functions are derived for designing the control parameters. The performances of fast regulation and high efficiency of the IPT converter system are verified using a prototype system.**

***Index Terms*—Control for maximum efficiency, inductive power transfer (IPT), wireless power transfer.**

I. Introduction

DESIGN and optimization of inductive power transfer (IPT) systems have been widely studied. One of the main objectives is to achieve high efficiency. The optimization involves the choice of appropriate structure of magnetic couplers [1] and their interoperability [2]. It is well known that a higher coupling coefficient and higher coil quality factors of the pair of windings of the magnetic coupler would increase the system efficiency [3], [4]. Optimization approaches for these two parameters to achieve high efficiency have been proposed [5], [6]. Meanwhile, since the system efficiency is not monotonically varying with the load, optimum loads that achieve maximum efficiency of the system are also studied [7]–[9]. Moreover, various design aspects to achieve maximum efficiency for different converter input–output transfer functions using series and parallel compensations have been studied [10], [11]. Previous studies show that given a coupling coefficient and coil quality factors, an IPT converter should be designed to operate at some fixed operating frequencies with load-independent transfer characteristic and slight modulation for soft switching when a simple half-bridge or full-bridge inverter circuit is used, and to operate within a restricted load range in order to achieve maximum efficiency [10]–[13]. Among the four basic types of compensation, the widely used *series–series* compensated IPT (SSIPT) converter is the most power efficient IPT converter when it is operating with load-independent output current [7]–[13]. However, in some practical applications, the design may not meet the required wide variations of the coupling coefficient, the load resistance, and the load power. Thus, once an IPT converter has been designed at a particular coupling coefficient and a particular load, the efficiency of the IPT system cannot always be maintained near its maximum point.

To improve the system efficiency under variation of the load, a load-side dc/dc converter is connected between the load and the secondary of an SSIPT converter to adaptively control the equivalent load observed by the SSIPT converter, thus maintaining a maximum efficiency of the front-end power amplifier driver [14], [15]. To achieve output regulation, source modulation is needed. The modulation can be provided by either a pulse width modulated inverter, a front-side dc/dc converter which amplitude modulates the inverter circuit, or a power amplifier. The inverter circuit is mostly implemented by either a half-bridge or full-bridge circuit, which provides the highest efficiency but suffers from shallow modulation due to the need for maintaining soft switching [9]–[11]. The depth of modulation can be greatly improved when the inverter is amplitude modulated by a front-end dc/dc converter. The combined circuit incurs a penalty of additional loss due to the extra power stage. The power amplifier can be considered as a circuit consisting of a front-side dc/dc converter, amplitude modulating an inverter circuit, with an output filter. The study by Li *et al.* [16] shows that a system consisting of an SSIPT converter with front-side and load-side dc/dc converters (the system is denoted as F-SSIPT-L) can achieve better overall system efficiency compared to a system consisting of the same SSIPT converter and a load-side dc/dc converter utilizing the modulation of the internal inverter (such a system is denoted as M-SSIPT-L) with frequency modulation. A maximum efficiency tracking (MET) algorithm has been proposed by Li *et al.* [16], where the secondary dc/dc converter regulates the output voltage while the front-side dc/dc converter maximizes the system efficiency. Another MET algorithm has also been studied using the F-SSIPT-L system where the front-side dc/dc converter controls the input current of the SSIPT converter for better handling of small coupling

Manuscript received December 9, 2016; revised April 3, 2017 and May 25, 2017; accepted June 27, 2017. Date of publication July 7, 2017; date of current version February 1, 2018. This work was supported by Hong Kong Polytechnic University under Central Research Grant G-YBKC. Recommended for publication by Associate Editor C. T. Rim. *(Corresponding author: S.-C. Wong.)*

The authors are with the Department of Electronic and Information Engineering, The Hong Kong Polytechnic University, Kowloon, Hong Kong (e-mail: zhicong.huang@connect.polyu.hk; enscwong@polyu.edu.hk; encktse@polyu.edu.hk).

Color versions of one or more of the figures in this paper are available online at http://ieeexplore.ieee.org.

Digital Object Identifier 10.1109/TPEL.2017.2724039

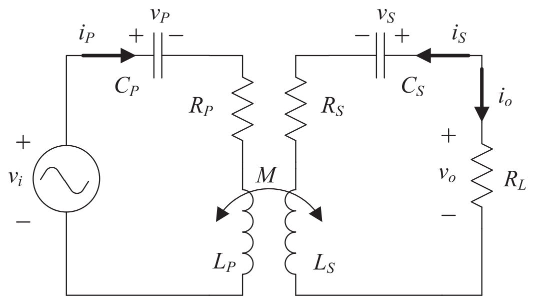

Fig. 1. IPT converter model.

coefficient and light load [17]. Furthermore, an MET algorithm has been applied to the inverter to minimize the input power of an M-SSIPT-L system where the load-side dc/dc converter solely regulates the output [18]. The benefit is that no wireless data feedback is needed from the secondary to the primary of the magnetic coupler. The MET control schemes studied so far are based on perturbation and observation (P&O) of the system power or the system efficiency [15]–[18]. It is well known that P&O-based control schemes are slow due to the uncertainties of perturbation speed and amplitude. Moreover, such control schemes are based on real-time processing of both voltage and current for obtaining information of power or efficiency, resulting in high error of the processed information and necessitating the use of cost-ineffective current sensor(s). In this paper, a simple and fast voltage control scheme for achieving maximum efficiency of the SSIPT converter is proposed for applications requiring fast regulation of load powers, such as charging of electric vehicles [29]–[31] and biomedical implants [32], [33].

II. Maximum IPT Converter Efficiency and Voltage Ratio

Fig. 1 shows an equivalent circuit of a commonly used SSIPT converter model, where the magnetic coupler has self-inductances L_P and L_S, and mutual inductance M. The magnetic coupler is compensated by external series compensated capacitors C_P and C_S. Subscripts P and S indicate parameters on the primary and secondary sides, respectively, of the magnetic coupler. The circuit is simplified as being driven by an approximate equivalent ac voltage source v_i at a fundamental angular frequency ω modulated by the inverter. The output is usually rectified to drive a dc load with R_L being the ac equivalent resistance. Losses are modeled aggregately using equivalent series resistors R_P and R_S [10]. Resistor R_P includes losses from the primary windings and the inverter circuit, while resistor R_S includes losses from the secondary windings and the rectifier circuit.

This SSIPT model has been studied in [9]–[11] with converter efficiency η and transconductance G given as

$$\eta(\omega, R_L) = \frac{\omega^2 M^2 R_L}{|Z_S + R_L|^2 R_P + \omega^2 M^2 (R_S + R_L)}, \text{ and} \tag{1}$$

$$G(\omega) = \frac{i_o}{v_i} = \frac{j\omega M}{Z_P(Z_S + R_L) + \omega^2 M^2} \tag{2}$$

where $Z_P = j\omega L_P + \frac{1}{j\omega C_P} + R_P$ and $Z_S = j\omega L_S + \frac{1}{j\omega C_S} + R_S$ are the impedance of the primary resonator and the secondary resonator, respectively.

For simplicity, the SSIPT converter is normally designed to operate at the aligned resonant frequency, i.e., $\omega = \omega_P = \omega_S$, where $\omega_P = \frac{1}{\sqrt{L_P C_P}}$ and $\omega_S = \frac{1}{\sqrt{L_S C_S}}$ [9], [18]. As a result, η in (1) is maximized at a particular load $R_{L,\mathrm{opt}}$, which can be calculated by solving $\frac{\partial \eta}{\partial R_L} = 0$, i.e.,

$$R_{L,\mathrm{opt}} = R_S \sqrt{1 + \frac{\omega^2 M^2}{R_P R_S}} \tag{3}$$

$$\approx \omega M \sqrt{\frac{R_S}{R_P}} \text{ for } \frac{\omega^2 M^2}{R_P R_S} \gg 1. \tag{4}$$

The magnitude of the transconductance $|G|$ at this operating frequency is given by

$$|G| = \left|\frac{i_o}{v_i}\right| = \frac{\omega M}{R_P(R_S + R_L) + \omega^2 M^2} \tag{5}$$

for $\frac{\omega^2 M^2}{R_P R_S} \gg 1$ and $\frac{\omega^2 M^2}{R_P R_L} \gg 1$.

The magnitude of the voltage transfer ratio $|H|$ at maximum efficiency is thus given by

$$|H| = \left|\frac{v_o}{v_i}\right| = |G| \, R_{L,\mathrm{opt}} \approx \sqrt{\frac{R_S}{R_P}}. \tag{6}$$

From (6), it is possible to maintain a high IPT converter efficiency by controlling the converter voltage ratio at $|H| = \sqrt{\frac{R_S}{R_P}}$ against variation of the load.

III. SSIPT Converter Voltage Ratio Control

A general three-stage IPT system is shown in Fig. 2 [16]–[18]. The IPT system includes a front-side dc/dc converter, an SSIPT converter, and a load-side dc/dc converter. The operating frequency of the inverter is fixed at the resonant frequency to achieve maximum efficiency. The control functions of the three-stage system provide:

1) regulation to the output voltage or current; and
2) control for maximum efficiency of the SSIPT converter.

Three control schemes with control functions $V_{\mathrm{err}}(m_1)$, $\eta(m_1)$ and $P_{\mathrm{IN}}(m_1)$ are shown in Fig. 2 and compared in Table I, where m_1 is a modulation index of V_{IN}. The following advantages of our proposed linear control method can be readily observed.

1) The control function versus modulated index m_1 (e.g., duty cycle of the front-side converter) is monotonic with a well-defined control reference $V_{\mathrm{err}} = 0$ to minimize error voltage $V_{\mathrm{err}} = V_1 - \sqrt{\frac{R_P}{R_S}} V_2$, i.e., to achieve the desired $|H|$ in (6). With a proper design, a simple linear proportional integral (PI) controller can be implemented in either analog or digital form. This results in a faster response.
2) The sampled voltages can be used for the linear PI controller without further processing. This results in a faster and more accurate response. Moreover, no current sensor is required, and the system cost is lower.

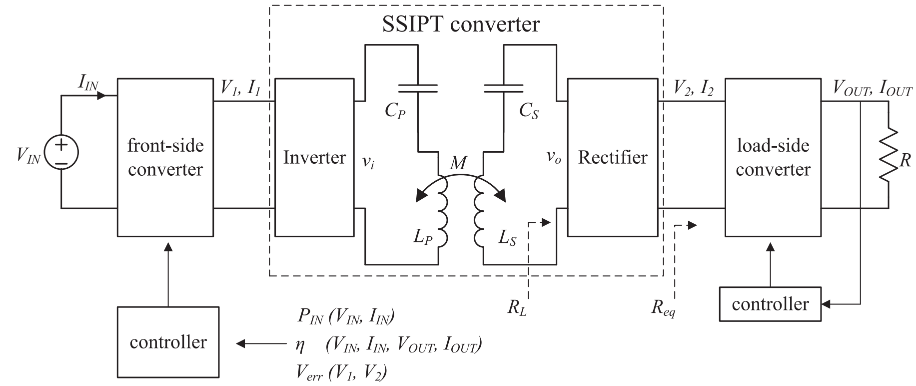

Fig. 2. SSIPT converter cascaded with a front-side converter and a load-side converter.

TABLE I
COMPARISON OF DIFFERENT CONTROL SCHEMES

Control function	V_{err}, voltage error control (this paper)	η, maximum efficiency tracking [16], [17]	P_{IN}, minimum input power tracking [18]
	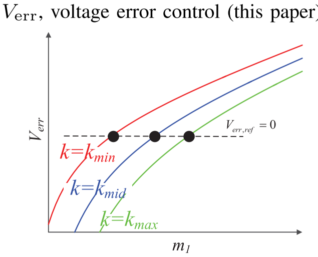	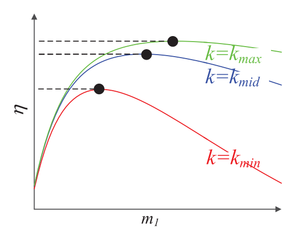	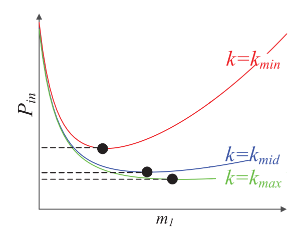
Monotonicity	$\frac{\Delta V_{\text{err}}}{\Delta m_1}$ is always positive	probing $\frac{\Delta \eta}{\Delta m_1}$ for signs	probing $\frac{\Delta P_{in}}{\Delta m_1}$ for signs
Control reference	$V_{\text{err,ref}} = 0$	adaptively tracking the maximum point.	adaptively tracking the minimum point.
Control method	PI controller, analog or digital	P&O, digital	P&O, digital
Sampling	V_1, V_2	$V_{\text{IN}}, I_{\text{IN}}, V_{\text{OUT}}, I_{\text{OUT}}$	$V_{\text{IN}}, I_{\text{IN}}$

The steady-state operation of the converter system is studied in this section. Small-signal analysis will be conducted in Section IV. The load-side converter regulates the output voltage or current so that the load appears as a power load P_O at the output of the SSIPT converter. Power balance requires that $P_O = V_2 I_2$. Substituting (5) and applying a scaling factor between square and sinusoidal magnitudes, we have $\frac{1}{\omega M} = \left|\frac{i_o}{v_i}\right| = \frac{\frac{\pi}{2} I_2}{\frac{4}{\pi} V_1}$, which gives

$$P_O = V_2 \frac{8}{\pi^2 \omega M} V_1. \tag{7}$$

To achieve (6), it is equivalent to minimize $|V_{\text{err}}|$ given by

$$V_{\text{err}} = V_1 - \sqrt{\frac{R_P}{R_S}} V_2 = V_1 - \sqrt{\frac{R_P}{R_S} \frac{P_O \pi^2 \omega M}{8}} \frac{1}{V_1}. \tag{8}$$

When using a front-side pulse width modulation (PWM) converter, V_1 is the modulated output of V_{IN} from modulation index $m_1 = \frac{V_1}{V_{\text{IN}}}$. Monotonic curves for the control function V_{err} of (8) are shown in Table I for various values of coupling coefficient $k = \frac{M}{\sqrt{L_P L_S}}$. A linear PI controller can be used for its simple structure, better robustness, and high reliability. The design will be presented in Section IV.

IV. CONTROLLER DESIGN

Linear PI controllers will be designed to optimize the efficiency of the SSIPT converter system. Fig. 3 shows a proposed schematic of control for the system. For the SSIPT converter, an H-bridge inverter is used to generate an ac voltage at the resonant frequency. Thus, the SSIPT converter behaves as a transconductance converter [11]. The current output is cascaded with a buck–boost converter, which is regulated with a standalone PI controller to generate a constant voltage output V_{OUT}. The front-side converter is a buck converter whose output voltage V_1 drives the SSIPT converter. Voltages V_1 and V_2 of the SSIPT converter are sampled. No current sensor is needed here. Voltage V_2 after being scaled by a factor of $\sqrt{\frac{R_P}{R_S}}$ is transmitted wirelessly from the secondary to the primary of the magnetic coupler and connected to the input of the PI controller of the buck converter. The voltage error V_{err} is nulled by the PI controller of the buck converter to achieve maximum efficiency of the SSIPT converter.

At the optimal efficiency point, steady-state parameters of the converters are calculated using $R_{\text{eq}} = \frac{\pi^2}{8} \omega M \sqrt{\frac{R_S}{R_P}}$, $R_{\text{buck}} = \frac{\pi^2}{8} \omega M \sqrt{\frac{R_P}{R_S}}$, $V_2 = V_{\text{OUT}} \sqrt{\frac{R_{\text{eq}}}{R}}$, and $V_1 = V_{\text{OUT}} \sqrt{\frac{R_{\text{buck}}}{R}}$. For

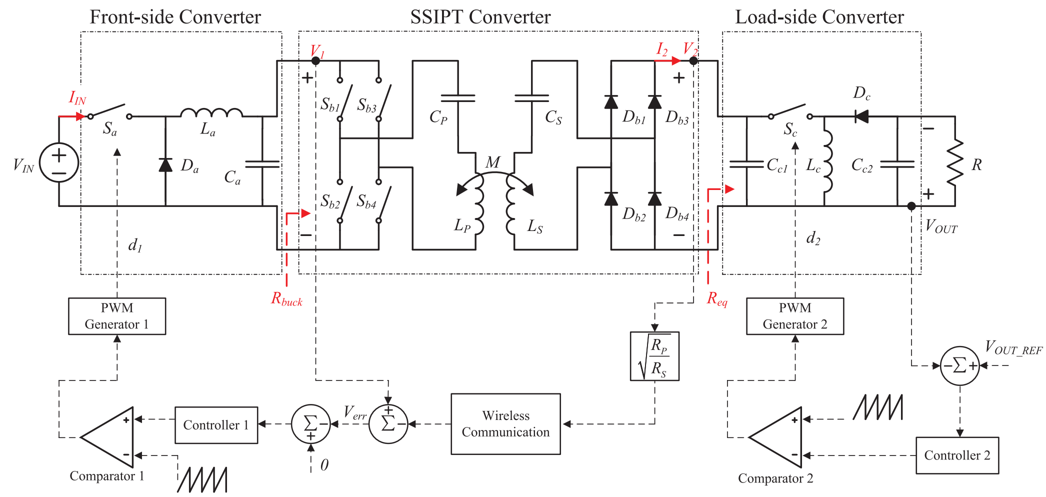

Fig. 3. Schematic of the system.

simplicity, the front-side and load-side converters are assumed lossless.

A. SSIPT Model

The small-signal transfer function of the SSIPT converter can be derived and calculated using the *generalized averaging technique* given in [19] and [20] for ordinary PWM and resonant power converters. Later, the same technique has been rephrased as *dynamic-phasor model* and applied for single-phase induction machines [21], microgrid systems [27], and extended for the predictive control of power converters [28]. Since the application of the generalized averaging technique or the dynamic-phasor model may not be obvious for IPT converters, the procedure is highlighted as follows. A sinusoidal signal $x(t)$ with time-varying magnitude X and phase angle θ can be written as

$$x(t) = X \sin(\omega t + \theta) \tag{9}$$

$$= X [\cos\theta \sin\omega t + \sin\theta \cos\omega t] \tag{10}$$

$$= X_d \sin\omega t + X_q \cos\omega t \tag{11}$$

$$= \Im\left((X_d + jX_q)e^{j\omega t}\right), \tag{12}$$

where $X_d = X\cos\theta$ and $X_q = X\sin\theta$ are the direct and quadrature components of $x(t)$, respectively. The time functions of the slow time-varying properties of X, θ, X_d, and X_q are omitted for brevity. It can be readily shown that

$$\frac{dx(t)}{dt} = \Im\left\{\left[\left(\frac{dX_d}{dt} - \omega X_q\right) + j\left(\frac{dX_q}{dt} + \omega X_d\right)\right]e^{j\omega t}\right\}. \tag{13}$$

For a pure capacitor C having current $i_C(t)$ and voltage $v_C(t)$, and a pure inductor L having current $i_L(t)$ and voltage $v_L(t)$, the following basic relationships hold:

$$i_C(t) = C\frac{dv_C(t)}{dt}, \text{ and} \tag{14}$$

$$v_L(t) = L\frac{di_L(t)}{dt}. \tag{15}$$

Substituting (12) and (13) into (14) and (15) and simplifying, we have

$$I_{C,d} + jI_{C,q} = C\left(\frac{dV_{C,d}}{dt} - \omega V_{C,q}\right) + j\left(\frac{dV_{C,q}}{dt} + \omega V_{C,d}\right), \text{ and} \tag{16}$$

$$V_{L,d} + jV_{L,q} = L\left(\frac{dI_{L,d}}{dt} - \omega I_{L,q}\right) + j\left(\frac{dI_{L,q}}{dt} + \omega I_{L,d}\right). \tag{17}$$

We can write $x(t)$ as a complex vector given as $\dot{X} = X_d + jX_q$. Hence, (16) and (17) can be simplified at steady state to become

$$\dot{I}_C = I_{C,d} + jI_{C,q} = j\omega\dot{V}_C, \text{ and} \tag{18}$$

$$\dot{V}_L = V_{L,d} + jV_{L,q} = j\omega\dot{I}_L \tag{19}$$

which is commonly used in complex vector analysis. Obviously, (16) and (17) are vector transformations of (14) and (15). We can write (16) and (17) in matrix forms as

$$\mathbf{I}_C = C\left(\mathbb{I}_\omega + \frac{d}{dt}\right)\mathbf{V}_C, \text{ and} \tag{20}$$

$$\mathbf{V}_L = L\left(\mathbb{I}_\omega + \frac{d}{dt}\right)\mathbf{I}_L \tag{21}$$

where $\mathbf{X}_Y = [X_{Y,d}, X_{Y,q}]^T$ is a column vector and

$$\mathbb{I}_\omega = \begin{pmatrix} 0 & -\omega \\ \omega & 0 \end{pmatrix} \tag{22}$$

is a 2×2 matrix.

The SSIPT system shown in Fig. 1 is governed by a state-space equation given as

$$\frac{d}{dt}X = AX + BV \tag{23}$$

where

$$X = \begin{bmatrix} v_P(t) & v_S(t) & i_P(t) & i_S(t) \end{bmatrix}^T \tag{24}$$

$$V = \begin{bmatrix} v_i(t) & v_o(t) \end{bmatrix}^T \tag{25}$$

$$A = \begin{bmatrix} 0 & 0 & \frac{1}{C_P} & 0 \\ 0 & 0 & 0 & \frac{1}{C_S} \\ -\alpha_P & \beta & -\alpha_P R_P & \beta R_S \\ \beta & -\alpha_S & \beta R_P & -\alpha_S R_S \end{bmatrix} \tag{26}$$

$$B = \begin{bmatrix} 0 & 0 & \alpha_P & -\beta \\ 0 & 0 & -\beta & \alpha_S \end{bmatrix}^T \tag{27}$$

$$\alpha_P = \frac{1}{L_P(1-k^2)} \tag{28}$$

$$\alpha_S = \frac{1}{L_S(1-k^2)} \tag{29}$$

$$\beta = \frac{k}{(1-k^2)\sqrt{L_P L_S}}. \tag{30}$$

Here, $v_P(t)$ is the voltage of C_P, $v_S(t)$ is the voltage of C_S, $i_P(t)$ is the current of L_P, and $i_S(t)$ is the current of L_S. The SSIPT system has input $v_i(t)$ and output $v_o(t)$ powering load R_L. All state variables are sinusoidal.

Equation (23) can be readily vector transformed using (20) and (21) to obtain

$$\frac{d}{dt}\mathbf{X} = \mathbf{AX} + \mathbf{BV} \tag{31}$$

where

$$\mathbf{X} = \begin{bmatrix} \mathbf{V_P} & \mathbf{V}_S & \mathbf{I}_P & \mathbf{I}_S \end{bmatrix}^T \tag{32}$$

$$\mathbf{V} = \begin{bmatrix} \mathbf{V_I} & \mathbf{V}_O \end{bmatrix}^T \tag{33}$$

$$\mathbf{A} = \begin{bmatrix} -\mathbb{I}_\omega & 0 & \frac{1}{C_P}\mathbb{I}_2 & 0 \\ 0 & -\mathbb{I}_\omega & 0 & \frac{1}{C_S}\mathbb{I}_2 \\ -\alpha_P\mathbb{I}_2 & \beta\mathbb{I}_2 & -\alpha_P R_P\mathbb{I}_2 - \mathbb{I}_\omega & \beta R_S\mathbb{I}_2 \\ \beta\mathbb{I}_2 & -\alpha_S\mathbb{I}_2 & \beta R_P\mathbb{I}_2 & -\alpha_S R_S\mathbb{I}_2 - \mathbb{I}_\omega \end{bmatrix} \tag{34}$$

$$\mathbf{B} = \begin{bmatrix} 0 & 0 & \alpha_P\mathbb{I}_2 & -\beta\mathbb{I}_2 \\ 0 & 0 & -\beta\mathbb{I}_2 & \alpha_S\mathbb{I}_2 \end{bmatrix}^T. \tag{35}$$

$\mathbb{I}_2$ is the two-dimensional identity matrix and variable $\mathbf{X}_Y = (X_{\mathrm{Yr}}, X_{\mathrm{Yi}})^T$.

A converter is cascaded with the SSIPT instead of a resistor. Assumed that the converter is well controlled to maintain a constant voltage or current output, it can be considered as a constant power load [22]. The extended describing function of $\mathbf{V}_O$ is given by

$$V_{O,d} = -2P_O \frac{I_{S,d}}{I_{S,d}^2 + I_{S,q}^2} \tag{36}$$

$$V_{O,q} = -2P_O \frac{I_{S,q}}{I_{S,d}^2 + I_{S,q}^2} \tag{37}$$

where P_O is the output power of the SSIPT. With (31), (36), and (37), the small-signal model of (31) can be derived as

$$\begin{cases} \dfrac{d}{dt}\hat{\mathbf{X}} = \hat{\mathbf{A}}\hat{\mathbf{X}} + \hat{\mathbf{B}}\hat{\mathbf{V}}_I \\ \hat{\mathbf{I}_O} = \hat{\mathbf{C}}\hat{\mathbf{X}} \end{cases} \tag{38}$$

where

$$\hat{\mathbf{X}} = \begin{bmatrix} \mathbf{V_P} & \mathbf{V}_S & \mathbf{I}_P & \mathbf{I}_S \end{bmatrix}^T \tag{39}$$

$$\hat{\mathbf{V}}_I = \begin{bmatrix} \mathbf{V_{I,d}} & \mathbf{V}_{I,q} \end{bmatrix}^T \tag{40}$$

$$\hat{\mathbf{I}_O} = \begin{bmatrix} \mathbf{I_{O,d}} & \mathbf{I}_{O,q} \end{bmatrix}^T \tag{41}$$

$$\hat{\mathbf{A}} = \begin{bmatrix} -\mathbb{I}_\omega & 0 & \frac{1}{C_P}\mathbb{I}_2 & 0 \\ 0 & -\mathbb{I}_\omega & 0 & \frac{1}{C_S}\mathbb{I}_2 \\ -\alpha_P\mathbb{I}_2 & \beta\mathbb{I}_2 & -\alpha_P R_P\mathbb{I}_2 - \mathbb{I}_\omega & \beta(R_S\mathbb{I}_2 + \mathbb{I}_\delta) \\ \beta\mathbb{I}_2 & -\alpha_S\mathbb{I}_2 & \beta R_P\mathbb{I}_2 & -\alpha_S(R_S\mathbb{I}_2 + \mathbb{I}_\delta) - \mathbb{I}_\omega \end{bmatrix} \tag{42}$$

$$\hat{\mathbf{B}} = \begin{bmatrix} 0 & 0 & \alpha_P\mathbb{I}_2 & -\beta\mathbb{I}_2 \end{bmatrix}^T \tag{43}$$

$$\hat{\mathbf{C}} = \begin{bmatrix} 0 & 0 & 0 & -\mathbb{I}_\omega \end{bmatrix} \tag{44}$$

$$\mathbb{I}_\delta = \begin{pmatrix} \mathrm{P} & -\mathrm{P} \\ \mathrm{P} & -\mathrm{P} \end{pmatrix} \text{ and} \tag{45}$$

$$\mathrm{P} = 2P_O \frac{-i_{S,d}^2 + i_{S,q}^2}{\left(i_{S,d}^2 + i_{S,q}^2\right)^2}. \tag{46}$$

The frequency response of the transconductance of the SSIPT converter is plotted using MATLAB with details shown in Fig. 4. We observe that within a bandwidth of one-hundredth of the fundamental frequency, the simulated transconductance can be approximated as an ideal transconductance $\frac{1}{\omega M}$, which is load independent.

B. Voltage Error Control Loop

We define $\hat{x}_y$ as the small-signal variable of X_y. Since the designed bandwidth of the control will be far lower than one-hundredth of the fundamental frequency, the SSIPT converter in Fig. 3 will be considered as a constant transconductance, given by

$$G_I = \frac{\hat{i}_2}{\hat{v}_1} = \frac{8}{\pi^2}\frac{1}{\omega M}. \tag{47}$$

General wireless communication protocols, such as 2.4G, are fast enough to transmit the output voltage V_2 of the SSIPT

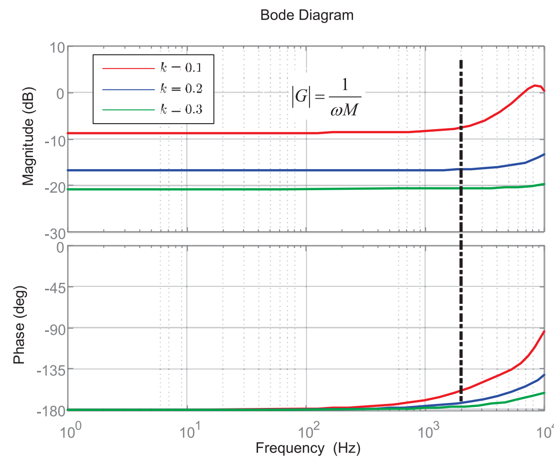

Fig. 4. Simulated frequency response of transconductance of the SSIPT model. Parameters used in simulation are: $L_P = L_S = 30\ \mu$H, $C_P = C_S = 21.11$ nF, $R_P = R_S = 0.5\ \Omega$, $\frac{\omega}{2\pi} = 200$ kHz, $v_i = 30$ V, and $P_O = 60$ W.

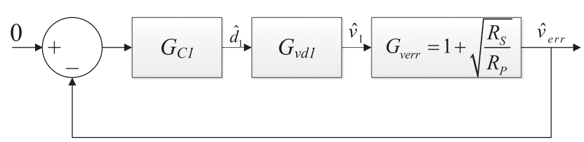

Fig. 5. Block diagram of the voltage control loop of the cascaded buck-SSIPT converter system.

converter, and the time delay is not considered here [3]. The load-side buck–boost converter is assumed to be ideally controlled as a constant power load, its small-signal input impedance is considered as a negative resistance $-R_{\text{eq}}$ in this small-signal model [22]. Voltage $\hat{v}_2$ is, thus, given as

$$\hat{v}_2 = \hat{v}_1 G_I(-R_{\text{eq}}) = -\hat{v}_1\sqrt{\frac{R_S}{R_P}}. \tag{48}$$

From (6) and the bandwidth considered, the voltage error transfer function of the SSIPT converter is assumed as

$$G_{\text{verr}} = \frac{\hat{v}_1 - \hat{v}_2}{\hat{v}_1} = 1 + \sqrt{\frac{R_S}{R_P}}. \tag{49}$$

The input voltage $\hat{v}_1$ of the SSIPT converter is controlled by the front-side buck converter shown in Fig. 3, the control-to-output transfer function of the buck converter is given by [23]

$$G_{\text{vd1}} = \frac{\hat{v}_1}{\hat{d}_1} = \frac{V_{\text{IN}}}{L_a C_a s^2 + \frac{L_a}{R_{\text{buck}}} s + 1}. \tag{50}$$

The control loop of the system is shown in Fig. 5. The transfer function of the input duty cycle $\hat{d}_1$ to the voltage error $\hat{v}_{\text{err}}$ is given by $G_{\text{vd1}} G_{\text{verr}}$, of which the Bode diagram is shown in Fig. 6(a). For this system, the design of the compensator G_{C1} is similar to that of a buck converter [24]. Thus, a simple PI controller G_{C1} can be chosen as

$$G_{C1} = \frac{K_P s + K_I}{s}. \tag{51}$$

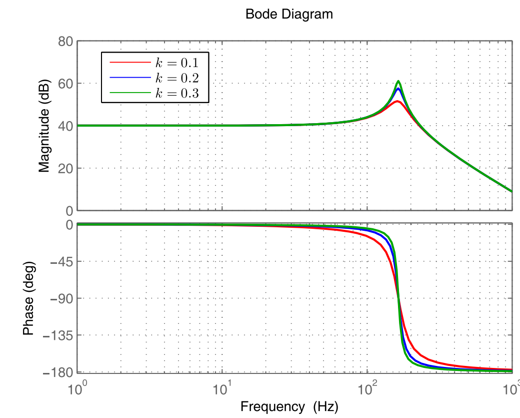

(a)

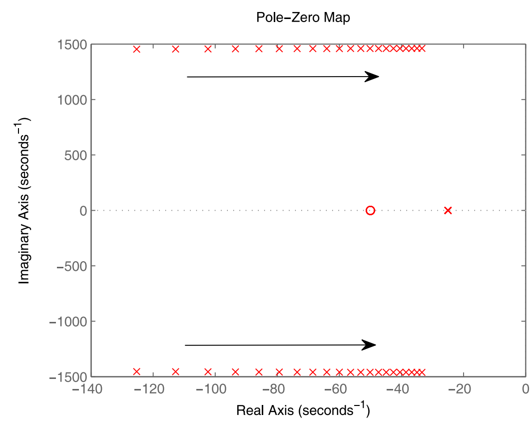

(b)

Fig. 6. Small-signal characteristics of the buck-SSIPT converter. Simulation parameters of the SSIPT converter are $L_P = L_S = 30\ \mu$H, $C_P = C_S = 21.11$ nF, and $\frac{\omega}{2\pi} = \frac{\omega_P}{2\pi} = \frac{\omega_S}{2\pi} = 200$ kHz. Parameters of the buck converter are $L_a = 1.2$ mH, $C_a = 760\ \mu$F, $V_{\text{IN}} = 50$ V, $V_O = 30$ V, and $R = 20\,\Omega$. (a) Frequency response of $\hat{v}_{\text{err}}$ versus $\hat{d}_1$. (b) Locations of pole (marked with "x") and zero (marked with "o") of the buck-SSIPT converter with $K_P = 0.01$, $K_I = 0.5$, when k increases from 0.1 to 0.3 as indicated by the arrow direction.

C. Stability Analysis

The open-loop transfer function T of the front-side buck converter cascaded with the SSIPT converter (buck-SSIPT converter) is given by

$$T = G_{C1} G_{\text{vd1}} G_{\text{verr}}. \tag{52}$$

By substituting (49), (50), and (51) into (52) and putting $1 + T = 0$, a third-order characteristic equation of the buck-SSIPT converter is obtained as

$$a_3 s^3 + a_2 s^2 + a_1 s + a_0 = 0 \tag{53}$$

where $a_3 = L_a C_a$, $a_2 = \frac{L_a}{R_{\text{buck}}}$, $a_1 = (1 + \sqrt{\frac{R_S}{R_P}}) K_P V_{\text{IN}} + 1$, and $a_0 = (1 + \sqrt{\frac{R_S}{R_P}}) K_I V_{\text{IN}}$.

The load R and the coupling coefficient k usually vary within some ranges during operation. For stable control, K_P and K_I should be designed to ensure system stability for the whole operating range. From the characteristic equation, R does not

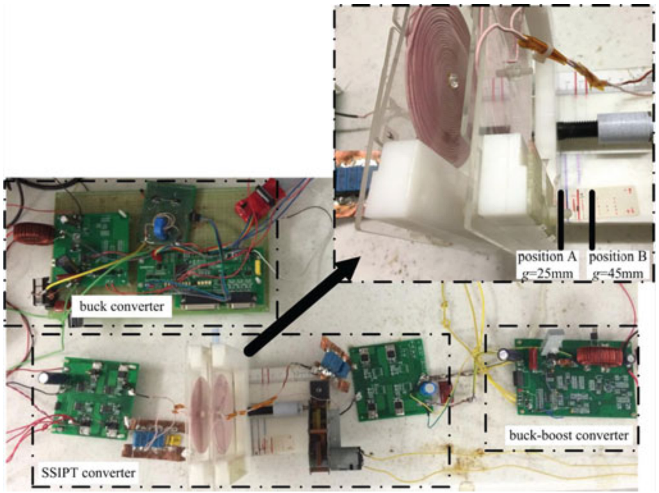

Fig. 7. Experiment setup of the system and enlarged image of the loosely coupled transformer.

contribute to the design of K_P and K_I. An example design of the controller shown in Fig. 6(b) illustrates that all roots locate on the left-half plane. Therefore, the stability of the system is ensured for k varying from 0.1 to 0.3.

V. Experimental Verification

An experimental prototype as shown in Fig. 7 is built to verify the linear control scheme and a version of P&O control scheme [18] is also implemented for comparison. The parameters of the schematic shown in Fig. 3 are given in Table II.

A. Design of Control Parameters

When the magnetic coupler is designed without a magnetic core, the variation of the air gap distance has little effect on the self-inductances. Thus, the resonant frequency can be considered as constant and the operating frequency of the inverter can be fixed. However, when the magnetic coupler is designed with a magnetic core to improve the coupling coefficient, the variation of the air gap distance will affect the self-inductances significantly [25]. Therefore, the operating frequency of the inverter should be dynamically adjusted to match the resonant frequency by using additional control, such as the self-oscillating control given in [26]. For the prototype studied in this paper, since the magnetic coupler is designed without a magnetic core, the variation of the air gap distance has little effect on the self-inductances, as shown in Table II, and no additional control for frequency adaptation is applied. The input voltage V_{IN} of this prototype is fixed at 50 V. The output voltage V_{OUT} is maintained at 30 V. A PI controller with $K_P = 0.01$ and $K_I = 0.5$ is designed for voltage control.

The SSIPT converter is designed to operate at zero input-phase angle. Apart from the winding loss, additional loss to be incorporated into R_P from the inverter includes conduction loss from R_{on} and turn-on loss $P_{\text{switch-on}}$ of the MOSFET switches. Additional loss to be incorporated into R_S includes loss due to the rectifier forward voltage V_F. Therefore, R_P and R_S in (6) are approximated as $R_P \approx R_{P,w} + 2R_{\mathrm{on}} + \frac{16P_{\text{switch-on}}}{\pi^2 I_1^2}$ and $R_S \approx R_{S,w} + \frac{16V_F}{\pi^2 I_2}$, where $R_{P,w}$ and $R_{S,w}$ are the primary and secondary winding resistances, respectively, of the magnetic coupler.

The efficiency of the SSIPT converter is measured by a Yokogawa PX8000 Precision Power Scope. The buck–boost converter is closed-loop controlled and the buck converter is also closed-loop controlled with different control references. The efficiency curves of the SSIPT converter versus output power for different values of the voltage ratio are measured as shown in Fig. 8. At $\frac{V_2}{V_1} = 1$, near maximum efficiency (with less than 1% error) can be achieved under different loading conditions. Therefore, $\frac{V_2}{V_1} = 1$ is used as the control reference for achieving maximum efficiency.

B. Small-Signal Response

Fig. 9 shows the measured frequency response of the input duty cycle to the voltage error of the SSIPT converter. It matches the simulation result shown in Fig. 6(a) and verifies that the design of small-signal parameters of the controller for the cascaded buck-SSIPT converter can follow that of a buck converter.

C. Transient Response Against Variation of k

To show the performance of the proposed control, variation of the air gap distance is introduced by using a DC motor which dynamically varies the position of the secondary-side coupler. In Fig. 7, an enlarged image shows the prototype of the loosely coupled transformer with position variation driven by a motor. At position A, the air gap distance g is 25 mm and the coupling coefficient k is 0.2541. At position B, g is 45 mm and the coupling coefficient k is 0.1217. More parameters of the loosely coupled transformer are shown in Table II.

Experimental waveforms using voltage error control for the dynamical variation of g at a time scale of 2 s/div are shown in Fig. 10. The efficiency of the system is kept at its optimum by observing that the instantaneous voltages V_2 and V_1 are kept almost identical under variation of k (or g).

As a comparison, experimental waveforms using an implementation of the minimum input current P&O control are also measured as shown in Fig. 11. The same variation speed of g as in Fig. 10 is used. In the minimum input current P&O control, a perturbation frequency 20 times faster than that adopted in [18] is used with the same perturbation size. Thus, the P&O control in this paper is theoretically faster than that in [18]. Fig. 11 shows that, the instantaneous input current I_{IN} needs more than 8 s to settle to the steady-state solution. The response of this P&O control is much slower than the voltage error control proposed in this paper against variations of k.

D. Transient Response Against Load Variations

Fig. 12 shows the waveforms of voltage tracking processes of the load R switching from 55 to 10 Ω and from 10 Ω back to 55 Ω. Using the PI controller, the steady-state error is eliminated. Within 300 ms, the input voltage V_1 and the output voltage V_2 are tracked, so that maximum efficiency of the system is

TABLE II
COMPONENTS AND PARAMETERS OF THE SYSTEM

Converter	Parameters	Symbol	Value		
Buck	Switch	S_a	IRF540N		
	Diode	D_a	MBR20100CTG		
	Inductor	L_a	1.2 mH		
	Capacitor	C_a	780 μF		
SSIPT	Switches	S_{b1}-S_{b4}	MTP5P06V		
	Diode	D_{b1}-D_{b4}	MBR20100CTG		
	Inner diameter	d_i	9 mm		
	Coil width	w	1.2 mm		
	Outer diameter	d_o	88 mm		
	Primary turns	N_P	29		
	Secondary turns	N_S	30		
	Air gap distance	g	45 mm	33 mm	25mm
	Coupling coefficient	k	0.1217	0.1739	0.2541
	Primary self inductance	L_P	31.48 μH	31.477 μH	31.467 μH
	Secondary self inductance	L_S	32.98 μH	32.974 μH	32.955 μH
	Primary winding resistance	$R_{P,w}$	245.8 mΩ	245.76 mΩ	245.59 mΩ
	Secondary winding resistance	$R_{S,w}$	246.3 mΩ	246.32 mΩ	246.33 mΩ
	Compensation capacitance	C_P	19.98 nF		
	Compensation capacitance	C_S	19.08 nF		
Buck-boost	Switch	S_c	IRF540N		
	Diode	D_c	MBR20100CTG		
	Capacitor	C_{c1}	680 μF		
	Inductor	L_c	1.2 mH		
	Capacitor	C_{c2}	470 μF		

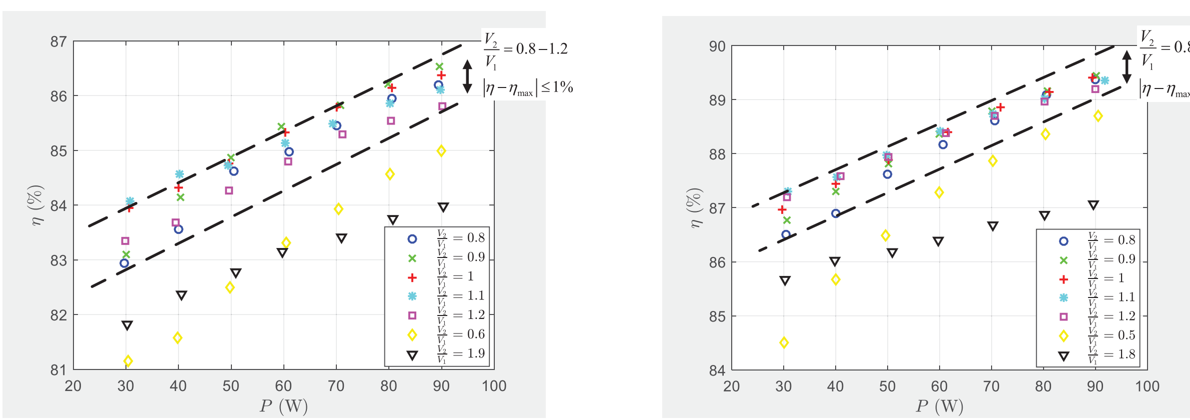

(a) (b)

Fig. 8. Measured efficiency of the SSIPT converter versus output power under various voltage gains at (a) $k = 0.1739$, (b) $k = 0.2541$.

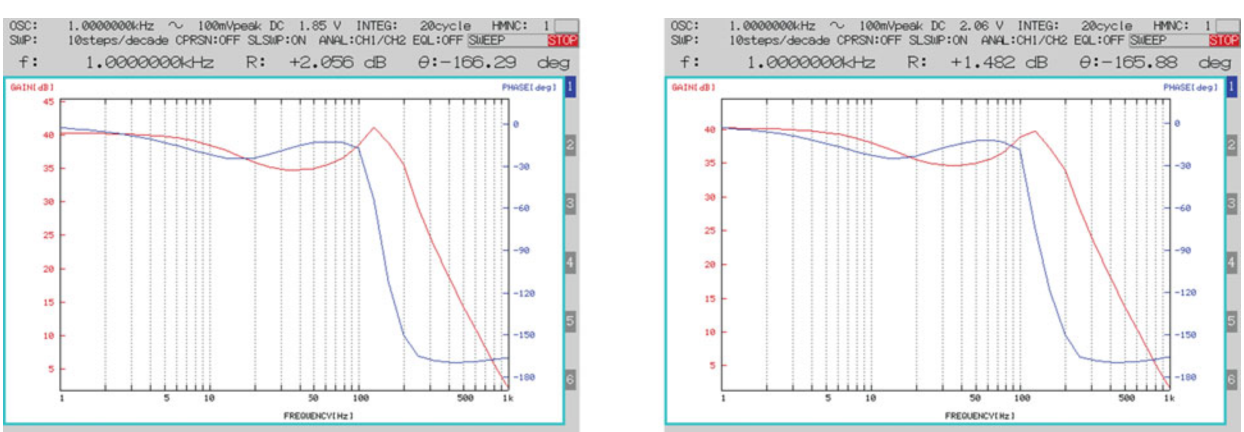

(a) (b)

Fig. 9. Measurements of the frequency response of input duty cycle to voltage error of the SSIPT at (a) $k = 0.1739$, (b) $k = 0.2541$.

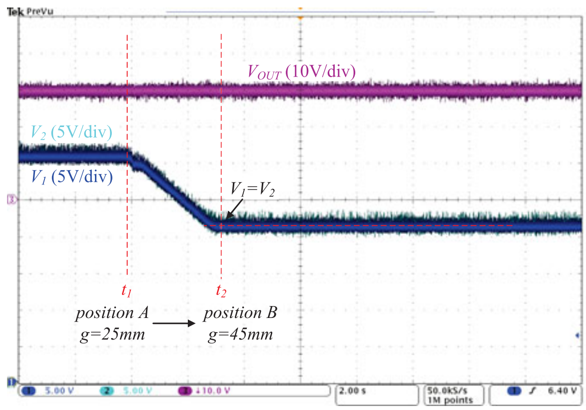

(a)

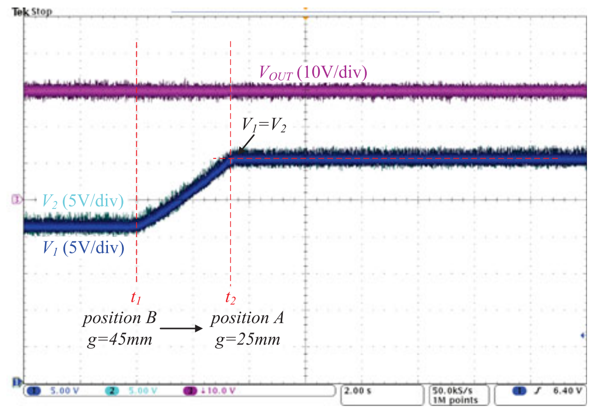

(b)

Fig. 10. Transient waveforms of key control parameters of voltage error control with g dynamically changing (a) from 25 to 45 mm, and (b) from 45 mm back to 25 mm. The load resistance R is 10 Ω.

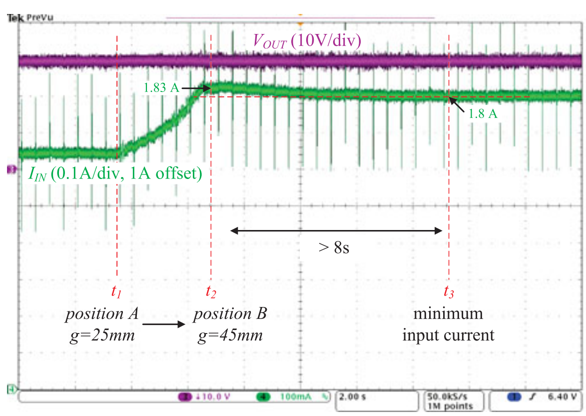

(a)

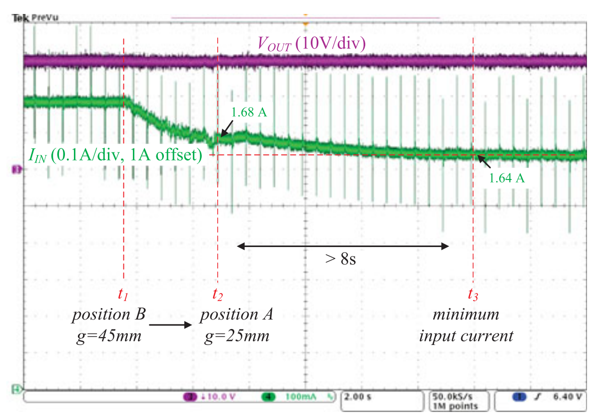

(b)

Fig. 11. Transient waveforms of key control parameters of an implementation of the minimum input current P&O control with g dynamically changing (a) from 25 to 45 mm, and (b) from 45 mm back to 25 mm. The loading condition is $R = 10\ \Omega$.

maintained. We have performed experiments using the same parameters based on the P&O control implemented in Section V-C. We found that the transient voltage fluctuations can be harmful to the converters. Therefore, a reduced load range switching from 30 to 10 Ω is used for comparison of performance between the voltage error control and the P&O control. Four key parameters $I_{\rm IN}$, V_1, V_2, and $V_{\rm OUT}$ of the system, as shown in Fig. 3, are chosen for the comparison of waveforms. In Fig. 13, the time base is set at 4 s/div, the test systems are open loop before t_1 with $R = 30\ \Omega$, the controls are applied after t_1, and the loads are switched to $R = 10\ \Omega$ at t_2.

Fig. 13(a) shows the transient waveforms when the voltage error control is used. It can be observed that $V_{\rm OUT}$ is always tightly regulated regardless of the excitations applied. This shows that the independently controlled load-side buck–boost converter can be stable with the input current I_2 (not shown) and voltage V_2 for the whole period of time indicated in Fig. 13(a). As soon as the voltage ratio control is applied at t_1, V_2/V_1 is immediately regulated at 1. At the same time, $I_{\rm IN}$ is also reduced immediately, thus improving the system efficiency. At t_2, the output power increases by threefold by switching the load resistance from 30 to 10 Ω. The voltage ratio is rapidly followed and controlled with $V_1 = V_2 = 30$ V at steady state.

Under the same experimental condition, the minimum input current P&O control produces the transient waveforms shown in Fig. 13(b). The system is completely out of control after t_2 upon load switching. The system instability can be explained as follows. With the same initial condition as that of the voltage ratio control, the minimum input current P&O control is executed right after t_1. It takes more than 10 s to search for the minimum input current. As shown in Fig. 13(b), the voltage ratio V_2/V_1 can be kept between 0.8 and 1.2, which are within the range of maximum efficiency as indicated in Fig. 8. At t_2, the output power increases three times by switching the load resistance from 30 to 10 Ω. The SSIPT converter is a transconductance converter and the load-side converter is a current-driven converter. The output current I_2 of the SSIPT converter is proportional to V_1. Due to the slow regulation of V_1 by the P&O control, I_2 cannot keep up with the sudden large increment of the output power. However, the control loop of the load-side converter is fast. Therefore, the voltage input V_2 of the current-driven load-side converter rises rapidly trying to acquire more power. As shown in Fig. 13(b),

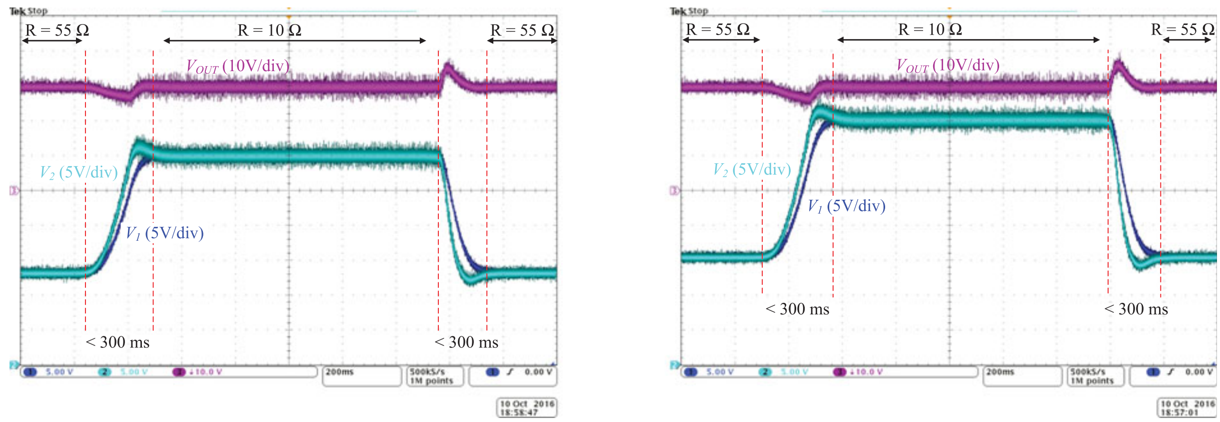

(a) (b)

Fig. 12. Transient waveforms of voltage tracking processes for R switching from 55 to 10 Ω and from 10 to 55 Ω at (a) $k = 0.1739$, (b) $k = 0.2541$.

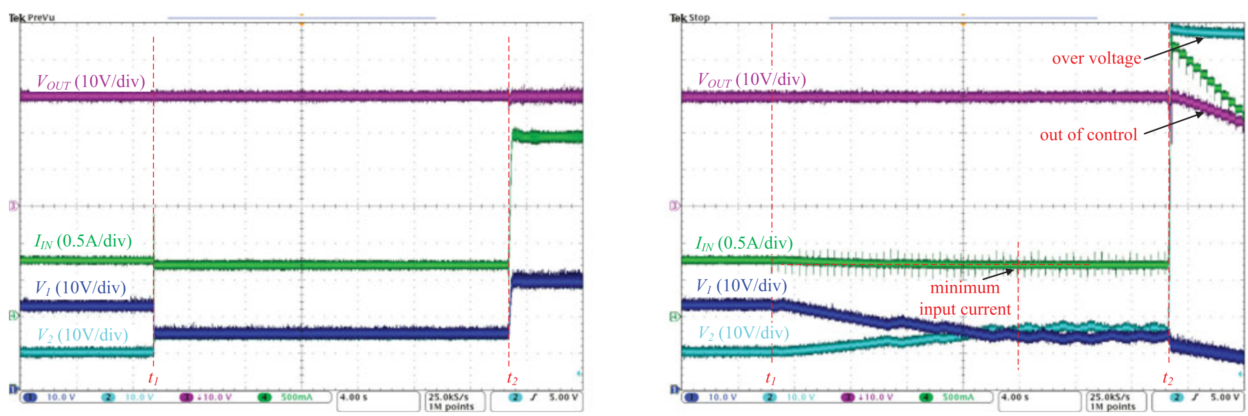

(a) (b)

Fig. 13. Transient waveforms of (a) voltage error control and (b) minimum input current P&O control. At t_1, the control is executed. At t_2, load resistance R is switched from 30 to 10 Ω. k is 0.1739.

TABLE III
k-INDEPENDENT CONVERTER TRANSFER FUNCTION AT MAXIMUM EFFICIENCY

Topology	Converter at maximum efficiency
SS	$\frac{v_o}{v_i} = \sqrt{\frac{R_S}{R_P}}$
PS	$\frac{v_o}{i_i} = \omega L_S \sqrt{\frac{R_S}{R_P}}$

V_2 becomes saturated because of over voltage, leading to the output voltage being out of control. By comparing Fig. 13(a) and (b), the voltage error control has better robustness against load variation due to its faster regulation speed.

E. Discussion

For an IPT converter with a k-independent input-to-output transfer function and maximum efficiency, the linear control method proposed in this paper can be used. Two example converters are shown in Table III. The voltage input SS-topology is chosen as the example converter of the system. For IPT converters having k-dependent input-to-output transfer functions and maximum efficiency, before applying this linear control method, the k-dependent characteristic should be removed by some means, such as using a self-oscillating control as proposed in [26]. Design parameters of the IPT converters are usually known during the design phase. Equivalent series resistances R_P and R_S can be estimated from device parameters. The approximated voltage ratio V_2/V_1 can be calculated using (6) as a control reference. Moreover, if the parameters are not available during the design phase or whenever verification is necessary, they can be measured experimentally as illustrated in Fig. 8. Alternatively, automatic in-circuit measuring methods, such as the P&O method, can also be implemented to determine the voltage ratio V_2/V_1 at maximum efficiency dynamically at the expense of using more sensors. The voltage ratio V_2/V_1 determined can be stored as a control reference for the linear control method proposed in this paper to improve performance.

VI. Conclusion

To achieve maximum efficiency of an IPT system, it is common to use nonlinear P&O control for an IPT system consisting of an IPT converter cascaded with front-side and load-side dc/dc converters. The P&O control is inevitably slow. A linear control scheme is proposed to achieve fast MET for an IPT system in this paper. By observing that the maximum efficiency occurs at a specific input-to-output voltage transfer ratio, a small-signal model for the IPT converter and the front-side converter operating as a combined transconductance converter is developed in this paper. To be compatible with the current output of the transconductance converter, the load-side converter is designed with a standalone transresistance converter. The controllers for the system are analyzed and experimentally verified to be fast and effective in this paper.

References

[1] M. Budhia, G. A. Covic, and J. T. Boys, "Design and optimization of circular magnetic structures for lumped inductive power transfer systems," *IEEE Trans. Power Electron.*, vol. 26, no. 11, pp. 3096–3108, Sep. 2011.

[2] W. Zhang, J. C. White, A. M. Abraham, and C. C. Mi, "Loosely coupled transformer structure and interoperability study for EV wireless charging systems," *IEEE Trans. Power Electron.*, vol. 30, no. 11, pp. 6356–6367, Nov. 2015.

[3] S. Li and C. C. Mi, "Wireless power transfer for electric vehicle applications," *IEEE J. Emerg. Sel. Topics. Power Electron.*, vol. 3, no. 1, pp. 4–17, Mar. 2015.

[4] A. P. Sample, D. T. Meyer, and J. R. Smith, "Analysis, experimental results, and range adaptation of magnetically coupled resonators for wireless power transfer," *IEEE Trans. Ind. Electron.*, vol. 58, no. 2, pp. 544–554, Feb. 2011.

[5] M. Budhia, J. T. Boys, G. A. Covic, and C. Y. Huang, "Development of a single-sided flux magnetic coupler for electric vehicle IPT charging systems," *IEEE Trans. Ind. Electron.*, vol. 60, no. 1, pp. 318–328, Jan. 2013.

[6] R. P. Wojda and M. K. Kazimierczuk, "Winding resistance of litz-wire and multi-strand inductors," *IET Power Electron.*, vol. 5, no. 2, pp. 257–268, Feb. 2012.

[7] C. K. Lee, W. X. Zhong, and S. Y. R. Hui, "Effects of magnetic coupling of non-adjacent resonators on wireless power domino-resonator systems," *IEEE Trans. Power Electron.*, vol. 27, no. 4, pp. 1905–1916, Apr. 2012.

[8] S. Y. R. Hui, W. Zhong, and C. K. Lee, "A critical review of recent progress in mid-range wireless power transfer," *IEEE Trans. Power Electron.*, vol. 29, no. 9, pp. 4500–4511, Sep. 2014.

[9] W. Zhang, S. C. Wong, C. K. Tse, and Q. Chen, "Design for efficiency optimization and voltage controllability of series-series compensated inductive power transfer systems," *IEEE Trans. Power Electron.*, vol. 29, no. 1, pp. 191–200, Jan. 2014.

[10] W. Zhang, S. C. Wong, C. K. Tse, and Q. Chen, "Analysis and comparison of secondary series and parallel compensated inductive power transfer systems operating for optimal efficiency and load-independent voltage-transfer ratio," *IEEE Trans. Power Electron.*, vol. 29, no. 6, pp. 2979–2990, Jun. 2014.

[11] W. Zhang, S. C. Wong, C. K. Tse, and Q. Chen, "Load-independent duality of current and voltage outputs of a series or parallel compensated inductive power transfer converter with optimized efficiency," *IEEE J. Emerg. Sel. Topics. Power Electron.*, vol. 3, no. 1, pp. 137–146, Mar. 2015.

[12] X. Qu, H. Han, S. C. Wong, C. K. Tse, and W. Chen, "Hybrid IPT topologies with constant-current or constant-voltage output for battery charging applications," *IEEE Trans. Power Electron.*, vol. 30, no. 11, pp. 6329–6337, Nov. 2015.

[13] Z. Huang, S. C. Wong, and C. K. Tse, "Design of a single-stage inductive-power-transfer converter for efficient EV battery charging," *IEEE Trans. Veh. Technol.*, vol. 66, no. 7, pp. 5808–5821, Jul. 2017.

[14] M. Fu, C. Ma, and X. Zhu, "A cascaded boost-buck converter for high-efficiency wireless power transfer systems," *IEEE Trans. Ind. Informat.*, vol. 10, no. 3, pp. 1972–1980, Aug. 2014.

[15] M. Fu, H. Yin, X. Zhu, and C. Ma, "Analysis and tracking of optimal load in wireless power transfer systems," *IEEE Trans. Power Electron.*, vol. 30, no. 7, pp. 3952–3963, Jul. 2015.

[16] H. Li, J. Li, K. Wang, W. Chen, and X. Yang, "A maximum efficiency point tracking control scheme for wireless power transfer systems using magnetic resonant coupling," *IEEE Trans. Power Electron.*, vol. 30, no. 7, pp. 3998–4008, Jul. 2015.

[17] T. D. Yeo, D. Kwon, S. T. Khang, and J. W. Yu, "Design of maximum efficiency tracking control scheme for closed-loop wireless power charging system employing series resonant tank," *IEEE Trans. Power Electron.*, vol. 32, no. 1, pp. 471–478, Jan. 2017.

[18] W. X. Zhong and S. Y. R. Hui, "Maximum energy efficiency tracking for wireless power transfer systems," *IEEE Trans. Power Electron.*, vol. 30, no. 7, pp. 4025–4034, Jul. 2015.

[19] S. R. Sander, J. M. Noworolski, X. Z. Liu, and G. C. Verghese, "Generalized averaging method for power conversion circuits," *IEEE Trans. Power Electron.*, vol. 6, no. 2, pp. 251–259, Apr. 1991.

[20] S. C. Wong and A. D. Brown, "Analysis, modelling and simulation of series-parallel resonant mode converters," *IEEE Trans. Power Electron.*, vol. 10, no. 5, pp. 605–614, Sep. 1995.

[21] A. M. Stankovic, B. C. Lesieutre, and T. Aydin, "Modeling and analysis of single-phase induction machines with dynamic phasors," *IEEE Trans. Power Syst.*, vol. 14, no. 1, pp. 9–14, Feb. 1999.

[22] A. Emadi, A. Khaligh, C. H. Rivetta, and G. A. Williamson, "Constant power loads and negative impedance instability in automotive systems: Definition, modeling, stability, and control of power electronic converters and motor drives," *IEEE Trans. Veh. Technol.*, vol. 55, no. 4, pp. 1112–1125, Jul. 2006.

[23] R. Ahmadi, D. Paschedag, and M. Ferdowsi, "Closed-loop input and output impedances of DC-DC switching converters operating in voltage and current mode control," in *Proc. IEEE 36th Annu. Conf. IEEE Ind. Electron. Soc.*, Nov. 2010, pp. 2311–2316.

[24] W. R. Liou, M. L. Yeh, and Y. L. Kuo, "A high efficiency dual-mode buck converter IC for portable applications," *IEEE Trans. Power Electron.*, vol. 23, no. 2, pp. 667–677, Mar. 2008.

[25] M. Budhia, G. A. Covic, and J. T. Boys, "Design and optimization of circular magnetic structures for lumped inductive power transfer systems," *IEEE Trans. Power Electron.*, vol. 26, no. 11, pp. 3096–3108, Nov. 2011.

[26] L. Xu, Q. Chen, X. Ren, S. C. Wong, and C. K. Tse, "Self-oscillating resonant converter with contactless power transfer and integrated current sensing transformer," *IEEE Trans. Power Electron.*, vol. 32, no. 6, pp. 4839–4851, Jun. 2017.

[27] M. A. Elizondo, F. K. Tuffner, and K. P. Schneider, "Simulation of inrush dynamics for unbalanced distribution systems using dynamic-phasor models," *IEEE Trans. Power Electron.*, vol. 32, no. 1, pp. 633–642, Jan. 2017.

[28] S. Almér, S. Mariéthoz, and M. Morari, "Dynamic phasor model predictive control of switched mode power converters," *IEEE Trans. Control Syst.*, vol. 23, no. 1, pp. 349–356, Jan. 2015.

[29] G. A. Covic and J. T. Boys, "Modern trends in inductive power transfer for transportation applications," *IEEE J. Emerg. Sel. Topics. Power Electron.*, vol. 1, no. 1, pp. 28–41, Mar. 2013.

[30] S. Zhou and C. Chris Mi, "Multi-paralleled LCC reactive power compensation networks and their tuning method for electric vehicle dynamic wireless charging," *IEEE Trans. Ind. Electron.*, vol. 63, no. 10, pp. 6546–6556, Oct. 2016.

[31] J. M. Miller *et al.*, "Demonstrating dynamic wireless charging of an electric vehicle: The benefit of electrochemical capacitor smoothing," *IEEE Power Electron. Mag.*, vol. 1, no. 1, pp. 12–24, Mar. 2014.

[32] Q. Chen, S. C. Wong, C. K. Tse, and X. Ruan, "Analysis, design, and control of a transcutaneous power regulator for artificial hearts," *IEEE Trans. Biomed. Circuits Syst.*, vol. 3, no. 1, pp. 23–31, Feb. 2009.

[33] S. C. Tang, T. L. T. Lun, Z. Guo, K. W. Kwok, and N. J. McDannold, "Intermediate range wireless power transfer with segmented coil transmitters for implantable heart pumps," *IEEE Trans. Power Electron.*, vol. 32, no. 5, pp. 3844–3857, May 2017.

Zhicong Huang (S'14) received the B.Sc. degree in electrical engineering and automation and the M.Sc. degree in mechanical and electronic engineering, both from Huazhong University of Science and Technology, Wuhan, China, in 2010 and 2013, respectively. He is currently working toward the Ph.D. degree in power electronics at Hong Kong Polytechnic University, Kowloon, Hong Kong.

His current research interests include wireless power transfer and power electronics.

Siu-Chung Wong (M'01–SM'09) received the B.Sc. degree in physics from the University of Hong Kong, Hong Kong, in 1986, the M.Phil. degree in electronics from the Chinese University of Hong Kong, Hong Kong, in 1989, and the Ph.D. degree in electronic and computer engineering from the University of Southampton, Southampton, U.K., in 1997.

He joined the Hong Kong Polytechnic in 1988 as an Assistant Lecturer. From 2012 to 2015, he was appointed as a Chutian Scholar Chair Professor by the Hubei Provincial Department of Education, China, and the appointment was hosted by Wuhan University of Science and Technology, Wuhan, China. In 2013, he was appointed as the Guest Professor by the School of Electrical Engineering, Southeast University, Nanjing, China. He was a Visiting Scholar at the Center for Power Electronics Systems, Virginia Tech, VA, USA, in November 2008, at Aero-Power Sci-Tech Center, Nanjing University of Aeronautics and Astronautics, Nanjing, China, in January 2009, and the School of Electrical Engineering, Southeast University, Nanjing, China, in March 2012. He is currently an Associate Professor in the Department of Electronic and Information Engineering, The Hong Kong Polytechnic University, Hong Kong, where he conducts research in power electronics.

Dr. Wong is a member of the Electrical College, The Institution of Engineers, Australia. He is an Editor of the *Energy and Power Engineering Journal* and a member of the Editorial Board of the *Journal of Electrical and Control Engineering*. He serves as a Guest Associate Editor of the IEEE JOURNAL OF EMERGING AND SELECTED TOPICS IN POWER ELECTRONICS, Special Issue on Power Electronics for Biomedical Applications, 2014. He serves as an Associate Editor of the IEEE TRANSACTIONS ON CIRCUITS AND SYSTEMS II.

Chi K. Tse (M'90–SM'97–F'06) received the B.Eng. (Hons.) degree with first class honors in electrical engineering and the Ph.D. degree in electrical engineering from the University of Melbourne, Parkville, VIC, Australia, in 1987 and 1991, respectively.

He is presently a Chair Professor at the Hong Kong Polytechnic University, Hong Kong, with which he served as the Head of the Department of Electronic and Information Engineering from 2005 to 2012. He is an author/coauthor of 10 books, 20 book chapters, and more than 500 papers in research journals and conference proceedings, and holds 5 U.S. patents.

Dr. Tse received a number of research and industry awards, including Prize Paper Awards by the IEEE TRANSACTIONS ON POWER ELECTRONICS in 2001 and 2015, the RISP *Journal of Signal Processing* Best Paper Award in 2014, Best Paper Award by the *International Journal of Circuit Theory and Applications* in 2003, two Gold Medals at the International Inventions Exhibition in Geneva in 2009 and 2013, a Silver Medal at the International Invention Innovation Competition in Canada in 2016, and a number of recognitions by the academic and research communities, including honorary professorship by several Chinese and Australian universities, Chang Jiang Scholar Chair Professorship, IEEE Distinguished Lectureship, Distinguished Research Fellowship by the University of Calgary, Gledden Fellowship, and the International Distinguished Professorship-at-Large by the University of Western Australia. While with the Hong Kong Polytechnic University, he received the President's Award for Outstanding Research Performance twice, Faculty Research Grant Achievement Award twice, Faculty Best Researcher Award, and several teaching awards. He serves and has served as the Editor-in-Chief for the IEEE TRANSACTIONS ON CIRCUITS AND SYSTEMS II (2016–2017), the IEEE CIRCUITS AND SYSTEMS MAGAZINE (2012–2015), the Editor-in-Chief of the IEEE CIRCUITS AND SYSTEMS SOCIETY NEWSLETTER (since 2007), an Associate Editor for three IEEE journal/transactions, the Editor for the *International Journal of Circuit Theory and Applications*, and is on the editorial boards of a few other journals. He also serves as a panel member of Hong Kong Research Grants Council and NSFC, and a member of several professional and government committees.